52nd IEEE Conference on Decision and Control
December 10-13, 2013. Florence, Italy

Modeling of Human Driver Behavior via Receding Horizon and Artificial Neural Network Controllers

Hongchuan Wei*, Weston Ross*, Stefano Varisco†, Philippe Krief†, and Silvia Ferrari*

Abstract— **This paper presents a comparison of receding horizon and artificial neural network controllers for the modeling of human driver behavior during coupled lateral-longitudinal maneuvers. Driver models have been previously developed using control theoretic approaches, such as model predictive control, also known as receding horizon control, and have been shown capable of providing satisfactory vehicle control. However, these models tend to outperform human drivers, for example, due to maneuvers that require high-frequency driver compensation, counter-steering behaviors as required to maintain stability, or modeling errors. Furthermore, tuning these driver models to different drivers, automobiles, and road conditions, can be very challenging, and requires expert human intervention. This paper presents an artificial neural network controller that overcomes these limitations, and, by adapting to the experimental data obtained from the human driver, is capable of reproducing the driver behavior more closely and under a broader range of operating conditions. The receding horizon and neural network controllers are tested and compared to the response of a professional human driver on a closed-course track using data obtained using a high-fidelity Ferrari GT driving simulator. The results show that the artificial neural network outperforms the receding horizon controller in mimicking the response of the professional human driver.**

I. INTRODUCTION

To date, control theoretic approaches such as receding horizon control (RHC), also known as model predictive control (MPC), have been shown effective at capturing the behavior of human drivers for a given vehicle model, trajectory, and speed profile [1] [2] [3]. A structural-model approach, originally developed for pilots involved in flight control tasks, was first proposed in [3] to model the steering behavior of a driver in lane-keeping tasks on a curvy road. Falcone et. al [1] demonstrated the effectiveness of MPCs to control a ground vehicle in real time by successively linearizing the nonlinear model used by the MPC. An approach combing ANN with MPC was shown to compensate for non-linearities and modeling errors in [2]. The effectiveness of these MPC approaches, however, is highly dependent on the accuracy of the mathematical model used to represent the vehicle dynamics. Also, experimental studies show that these models tend to outperform human drivers, for example, during maneuvers that require high-frequency driver compensation, sharp turns that result in counter-steering behaviors and/or modeling errors [4], [5]. As a result, they may not always provide a close representation of a driver behavior or, alternatively, may require constant (expert) human intervention to closely match the model to different human drivers, automobiles, or road conditions.

This paper presents a comparison of receding horizon and artificial neural network controllers used to model human driver behavior during coupled lateral-longitudinal maneuvers. The artificial neural network controller (ANN) was found to outperform the receding horizon controller (RHC) in matching the human response, particularly under challenging operating conditions, such as counter-steering. The ANN controller benefits from learning from training data generated by a professional human driver because it can learn from dynamics that are not captured by physics based models used in receding horizon controllers.

While existing approaches may be suitable to applications involving feedback control of autonomous vehicles [1], the ANN approach presented in this paper is better suited to applications that require an accurate model of human driver behavior. Such a model may be implemented during a vehicle design phase to reduce manufacturing delivery times and costs or to better test the vehicle safety and performance through simulations before experimental testing begins. As a result, the ability of the model to capture the performance limitations and, possibly, the mistakes of a real human driver, is just as important as its ability to control the vehicle. This paper compares the response of the RHC and ANN controllers to the response of a professional human driver on a closed-course track in the Ferrari GT simulator.

The Ferrari GT driving simulator reproduces a representative environment for vehicle testing and evaluation. Through the simulator – which includes a 120-degree screen with a two-dimensional (2D) surface rendering of the track to scale – the professional driver is able to drive the same vehicle models used for virtual development (vehicle dynamics, virtual durability, and control system development), both in Software-in-the-Loop and Hardware-in-the-Loop layouts. The same simulated vehicle can be driven by the automatic feedback controller or by a professional human driver. The simulator also includes elements like the cockpit, realistic graphics, and sound, in order to provide the human driver with a highly realistic driving experience.

The paper is organized as follows. Section II presents a detailed description of the bicycle model used to develop the RHC-based human driver model (HDM). The lateral and longitudinal vehicle models are also described in Section II. Section III presents the problem formulation and assump-

*H. Wei, W. Ross and S. Ferrari are with the Laboratory for Intelligent Systems and Controls (LISC), Duke University, Durham, NC, 27708, USA {hw88,weston.ross,sferrari}@duke.edu

†S. Varisco and P. Krief are with Ferrari S.p.A, via Abetone Inf.re 4, 41053, Maranello, (MO), Italia stefano.varisco@ferrari.com

978-1-4673-5716-6/13/$31.00 ©2013 IEEE

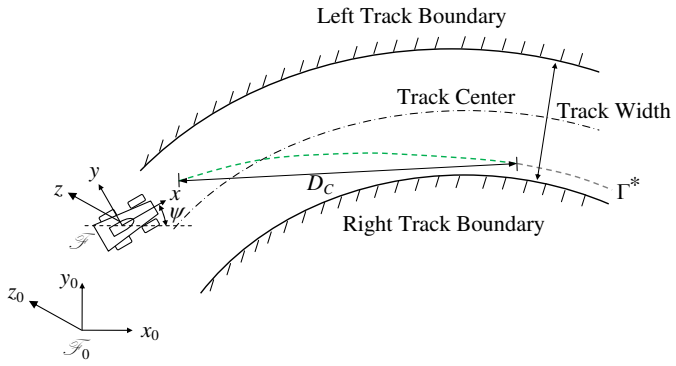

Fig. 1: Schematic diagram of the body frame of reference, $\mathscr{F}$, the inertial frame of reference, $\mathscr{F}_0$ and the track.

tions. The design of the RHC-based and ANN-based HDMs are presented in Section IV, and the results are presented in Section V.

II. Mathematical Models

This section presents the mathematical models used to represent the dynamic properties of the vehicle to be controlled for the RHC-based HDM design and simulations. The vehicle dynamics are derived using a moving frame and an inertial frame of reference, as shown in Fig. 1. The moving frame of reference, denoted by $\mathscr{F}$, is embedded in the vehicle, with the origin at the center of gravity, and such that the x-axis points in the direction of forward motion, the z-axis points upward, and the y-axis direction is chosen by the right-hand rule. The inertial frame of reference, denoted by $\mathscr{F}_0$, is fixed with respect to the track.

A. Model of Lateral Vehicle Dynamics

The lateral dynamics model is based on the bicycle model illustrated in Fig. 2, and taken from [6]. The equations of motion are derived by applying Newton's II Law in the y-direction, as follows,

$$m(\ddot{y}+\dot{\psi}\dot{x}) = F_{yr}+F_{yf}, \tag{1}$$

$$I_z\ddot{\psi} = aF_{yf}-bF_{yr}, \tag{2}$$

where a and b are the distances between the center of gravity and the front and rear wheels along the x-axis, respectively. The mass of the vehicle is denoted by m, and the moment of inertia of the vehicle with respect to the z-axis is denoted by I_z. The yaw angle, ψ, denotes the angle that the body x-axis makes with the inertial x_0-axis, and $\dot{\psi}$ denotes the yaw-rate. The front and rear lateral forces are modeled as linear functions of the front and rear slip angles α_f and α_r, respectively, such that,

$$F_{y_f} = K_f\alpha_f, \tag{3}$$

$$F_{y_r} = K_r\alpha_r, \tag{4}$$

where K_f and K_r are the front and rear tire cornering stiffness factor, respectively. The front and rear slip angles, α_f and α_r, are defined as the angles between a rolling wheel's

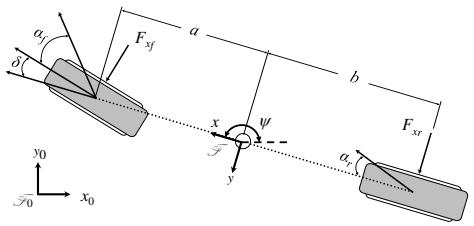

Fig. 2: Bicycle model.

actual direction of motion (x-axis) and the orientation of the wheel [7]. In addition to this definition, the front and rear relaxation lengths, l_f and l_r, are introduced to describe a first order delay to the change of slip angles, which increases the accuracy of the lateral dynamics model,

$$\frac{l_f}{\dot{x}}\dot{\alpha}_f+\alpha_f = \delta-\frac{a\dot{\psi}+\dot{y}}{\dot{x}}, \tag{5}$$

$$\frac{l_r}{\dot{x}}\dot{\alpha}_r+\alpha_r = \frac{b\dot{\psi}+\dot{y}}{\dot{x}}, \tag{6}$$

where δ denotes the angle of front tires with respect to x-axis, also known as, the steering angle [8].

As a result, the state-space representation of the lateral dynamic model is,

$$\dot{\mathbf{x}}_y = \mathbf{A}\mathbf{x}_y+\mathbf{B}\mathbf{u}_y, \tag{7}$$

where the lateral vehicle state is $\mathbf{x}_y = [y \quad \dot{y} \quad \dot{\psi} \quad \alpha_f \quad \alpha_r]^T$, the lateral control vector is $\mathbf{u}_y = [\delta]$, and the state-space matrices are defined as follows,

$$\mathbf{A} = \begin{bmatrix} 0 & 1 & 0 & 0 & 0 \\ 0 & 0 & -\dot{x} & K_f/m & K_r/m \\ 0 & 0 & aK_f/I_z & -bK_r/I_z & \\ 0 & -1/l_f & -a/l_f & -\dot{x}/l_f & 0 \\ 0 & -1/l_r & b/l_r & 0 & -\dot{x}/l_r \end{bmatrix}, \tag{8}$$

$$\mathbf{B} = [0 \quad 0 \quad 0 \quad \dot{x}/l_f \quad 0]^T. \tag{9}$$

B. Model of Longitudinal Vehicle Dynamics

The longitudinal vehicle dynamics are derived by applying Newton's II Law in the x-direction,

$$m\ddot{x} = 2F_{x_f}+2F_{x_r}-F_{aero}-R_{x_f}-R_{x_r}-mg\sin\theta, \tag{10}$$

where F_{x_f} and F_{x_r} are the tire forces generated by one front wheel or one rear wheel, respectively. F_{aero} is the aerodynamic drag force, R_{x_f} and R_{x_r} are the front and rear rolling resistances, respectively, and θ is the inclination angle of the road in the direction of the z-axis. The tire forces can be approximated by the Bakker-Nyborg-Pajecka (BNP) equations, as functions of the normal forces on the wheel and the tire slip ratio, σ_x,

$$\sigma_x = \begin{cases} \dfrac{r_w\omega_w-\dot{x}}{\dot{x}}, & \text{in braking mode,} \\ \dfrac{r_w\omega_w-\dot{x}}{r_w\omega_w}, & \text{in acceleration mode,} \end{cases} \tag{11}$$

where r_w denotes the effective rolling radius of the wheel, and ω_w is the angular velocity of the wheel.

The aerodynamic drag force is modeled as a quadratic function of the vehicle forward speed,

$$F_{aero} = \frac{1}{2}\rho C_d A_F \dot{x}^2, \tag{12}$$

where ρ is the mass density of air, C_d is the aerodynamic drag coefficient, and A_F is the frontal area of the vehicle, defined as the projected area of the vehicle in the direction of travel.

The rolling resistances, R_{x_f} and R_{x_r}, are assumed to be proportional to the normal force on the wheels,

$$R_{x_f} + R_{x_r} = \mu mg\cos\theta, \tag{13}$$

where μ is the rolling resistance coefficient, and g is the gravitational acceleration constant.

In order to relate the longitudinal vehicle dynamics to the engine torque and the brake pressure, the dynamics of the wheels are modeled as follows. For the front wheels, the rotational dynamics can be written as,

$$I_{w_f}\dot{\omega}_{w_f} = T_{w_f} - r_w F_{x_f} + P_b C_{b_f}, \tag{14}$$

where I_{w_f} is the rotational inertia of one front wheel, and $\dot{\omega}_{w_f}$ denotes the angular acceleration of the front wheels. P_b is the braking pressure acting on the wheel, and C_{b_f} is the front wheel braking coefficient that converts the braking pressure to a negative torque on the front wheels. T_{w_f} is the torque transmitted from the engine to the front wheel. Then, a first order differential equation is utilized to represent the response between the engine torque, T_e, and the front wheel torque, T_{w_f}, such that,

$$\tau\dot{T}_{w_f} + T_{w_f} = \frac{1}{2}\gamma C_{t_f} R T_e, \tag{15}$$

where γ is a driven mode indicator, which represents whether the vehicle is in a four-wheel-driven mode ($\gamma = 1$), or is in a rear-wheel-driven mode ($\gamma = 0$). τ is a time constant, R is the gear ratio, and C_{t_f} is the bias of front driven torque, that is, the percentage of engine torque distribution to the front wheels.

The dynamic equation for the rear wheels is similarly derived, such that,

$$I_{w_r}\dot{\omega}_{w_r} = T_{w_r} - r_w F_{x_r} + P_b C_{b_r}, \tag{16}$$

where T_{w_r} is the torque transmitted from the engine to the rear wheels. A first-order differential equation is also utilized to represent the response between the engine torque and the rear wheel torque,

$$\tau\dot{T}_{w_r} + T_{w_r} = \frac{C_{t_r}}{2(C_{t_r} - (C_{t_r} - 1)\gamma)} R T_e, \tag{17}$$

where $C_{t_r} = 1 - C_{t_f}$ is the bias of rear driven torque. Note that, as a manual vehicle, T_e and P_b cannot act on the wheel simultaneously. Thus, an additional constraint must be added to the model, such that $T_e P_b = 0$.

Letting the longitudinal state be defined as $\mathbf{x}_x = [\dot{x} \quad \omega_{w_f} \quad \omega_{w_r} \quad T_{w_f} \quad T_{w_r}]^T$, and the longitudinal control vector be defined as $\mathbf{u}_x = [T_e \quad P_b \quad \gamma]^T$, the nonlinear equation that governs the longitudinal dynamics is,

$$\dot{\mathbf{x}}_x = f(\mathbf{x}_x, \mathbf{u}_x), \tag{18}$$

where $f(\cdot,\cdot) : \mathbb{R}^5 \times \mathbb{R}^3 \to \mathbb{R}^5$, such that the vehicle longitudinal equations of motion are

$$\ddot{x} = 2\frac{F_{x_f} + F_{x_r}}{m} - \frac{\rho C_d A_F \dot{x}^2}{2m} - g(\cos\theta\mu + \sin\theta), \tag{19a}$$

$$\dot{\omega}_{w_f} = -\frac{1}{I_{w_f}}(r_w F_{x_f} + C_{b_f} P_b), \tag{19b}$$

$$\dot{\omega}_{w_r} = \frac{1}{I_{w_r}}(T_{w_r} - r_w F_{x_r} - C_{b_r} P_b), \tag{19c}$$

$$\dot{T}_{w_f} = -\frac{T_{w_f}}{\tau} + \frac{\gamma}{2\tau} C_{t_f} R T_e, \tag{19d}$$

$$\dot{T}_{w_r} = -\frac{T_{w_r}}{\tau} + \frac{\gamma C_{t_r}}{2(C_{t_r} - (C_{t_r} - 1)\gamma)} R T_e. \tag{19e}$$

The following sections present the RHC and the ANN human driver models obtained from the vehicle dynamics model described in this section. Their performance is compared to the response of a professional human driver in Section V.

III. PROBLEM FORMULATION

The problem addressed in this paper is to develop a human driver model that provides a mathematical description of a professional human driver behavior. The goal of the HDM is to generate control inputs that are as similar as possible to the control inputs of the human driver, when presented with the same road and vehicle conditions [9]. The input to the HDM is a subset of the information that the human driver can sense, which can be divided into two sets, the track information, $\mathbf{T}$, and the vehicle state, $\mathbf{x}$, comprised of lateral and longitudinal state variables, as well as vehicle information known to the driver (denoted by $\mathbf{x}_a$). The track information includes knowledge of the environment and consists of three parts: the target speed profile $\mathbf{V}^*$, the driver line Γ^*, and a portion of track ahead of the vehicle. The target speed profile determines the optimal speed along the track that the vehicle should follow, while the driver line determines the trajectory along the track that the vehicle should follow, specified by a preview distance D_c, which is obtained from a preview time, t_c,

$$D_c = t_c \dot{x}, \tag{20}$$

as shown in Fig. 1.

The dashed line in Fig. 1 represents the target future vehicle trajectory, also known as the driver line Γ^*. The green dashed line in Fig. 1 is the portion of the driver line that is available to the HDM at t_0. The target speed trajectory and the driver line are both used as inputs to the HDM because professional human drivers are well aware of the dynamic constraints of the vehicle, and can take them into account picking the optimal trajectory to follow, for example, in order to minimize the lap time in a given track. The track information, $\mathbf{T}$, also includes the portion of the track

immediately in front of the vehicle, which consists of the center line, track width, and the (black) track boundaries in Fig. 1. Since the target driver line is given to the controller, the track information is utilized mainly as a boundary that limits the error of the vehicle position with respect to the driver line, in the RHC design.

The vehicle state $\mathbf{x}$ represents the variables that a human driver can sense and that, in this paper, are assumed known without error. Thus, $\mathbf{x}$ is a fully-observable vehicle state vector that constitutes an input for the HDMs. It is comprised of the lateral vehicle state, $\mathbf{x}_y$, the longitudinal vehicle state, $\mathbf{x}_x$, and additional vehicle information, $\mathbf{x}_a$, which consists of the engine revolutions per minute (RPM), the current gear, and the lateral and longitudinal accelerations, such that,

$$\mathbf{x} = [\mathbf{x}_y^T \quad \mathbf{x}_x^T \quad \mathbf{x}_a^T]^T. \tag{21}$$

In the HDM design, it is also assumed that the vehicle has a manual transmission and that the vehicle dynamics, including the models of lateral and longitudinal tire forces, the gear ratio table, and the model of the maximum and minimum engine torques, are known.

Given the track information, the vehicle state, $\mathbf{x}$, and the dynamic constraints, the HDM computes an output vector, $\mathbf{u}$, that consists of the human driver control inputs to the vehicle. Thus, the output of the HDM consists of the lateral control and the longitudinal control,

$$\mathbf{u} = [\mathbf{u}_y^T \quad \mathbf{u}_x^T]^T. \tag{22}$$

The design of the HDM can be formulated as the following trajectory-following control problem. Given the track information, $\mathbf{T}$, and the vehicle state, $\mathbf{x}$, determine the control input to the vehicle, $\mathbf{u}$, such that the vehicle follows a known target speed profile, $\mathbf{V}^*$, and the driver line, Γ^*, subject to the dynamic constraints in (7), (18) while minimizing the cost function J_y. The trajectory-following control problem is approached using the RHC and ANN techniques described in the next section.

IV. METHODOLOGY

This section describes the designs for the RHC-based and ANN-based human driver models. Lateral and a longitudinal controllers are developed using the dynamical models described in Section II. Experimental data obtained from a professional human driving on the Ferrari GT vehicle simulator [10] is used to train the ANN. Both controllers are given identical information about vehicle state and target trajectories.

A. RHC-based HDM

This subsection describes the design of the RHC-based HDM. The principle of the RHC technique is shown in Fig. 3, where t_0 denotes the current time, t_c is the control horizon, and Δt is the sample time. RHC solves an optimal control problem over a fixed future interval $[t_0 \quad t_0 + t_c]$, given the current state $\mathbf{x}(t_0)$, and obtains an optimal control sequence $\mathbf{u}^*(t_0 + k\Delta t)_{k=0,\ldots,N-1}$, where $N = t_c/\Delta t$. Then, only the first input in the resulting optimal control sequence,

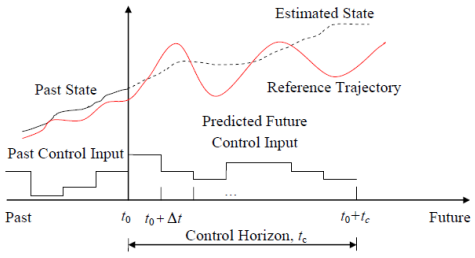

Fig. 3: Principle of receding horizon control.

namely $\mathbf{u}^*(t_0)$, is applied to the vehicle. The fixed horizon optimization is repeated at each sample time until the final time, t_f [11].

Figure 4 is a diagram of the RHC-based HDM, which consists of a lateral and a longitudinal receding horizon controller. For the lateral controller, the model of the plant is the time invariant linear system (7), with lateral state, $\mathbf{x}_y$, and lateral control, $\mathbf{u}_y$. By solving (7) and using the following relation [12], it is possible to estimate the sequence of future vehicle states,

$$\hat{\mathbf{x}}_y(t_0 + (k+1)\Delta t) = \mathbf{A_d}\hat{\mathbf{x}}_y(t_0 + k\Delta t) + \mathbf{B_d}\mathbf{u}_y(t_0 + k\Delta t), \tag{23}$$

which would progress from the sequence of future control inputs, where $\mathbf{A_d} = e^{\mathbf{A}\Delta t}$, and $\mathbf{B_d} = \int_0^{\Delta t} e^{\mathbf{A}t}dt$. The state space matrices $\mathbf{A_d}$ and $\mathbf{B_d}$ are assumed to be time-invariant over the sample time Δt.

Then, the estimated vehicle state is used to minimize a cost function, J_y, that represents the distance between $\mathbf{x}_y$, and a yaw angle reference trajectory generated by the human driver during field experiments, such that,

$$\begin{aligned} J_y(\mathbf{u}_y, \mathbf{x}_y(t_0), t_c) = \|[\hat{\psi}(t_0 + \Delta t) \quad \ldots \quad \hat{\psi}(t_0 + N\Delta t)] \\ - [\psi^*(t_0 + \Delta t) \quad \ldots \quad \psi^*(t_0 + N\Delta t)]\|_2, \end{aligned} \tag{24}$$

where $\|\cdot\|_2$ denotes the L^2 norm.

The lateral controller also considers the constraint imposed on the vehicle by the track boundaries, which can each be approximated by a third-order polynomial function defined with respect to the body frame, $\mathscr{F}$ [13]. The two polynomial functions for the boundaries to the left and right of the vehicle are denoted by $y = h_l(x)$ and $y = h_r(x)$, respectively, and their coefficients are determined by a curve-fitting algorithm, at each sample time. Therefore, the track-boundaries constraints can be expressed as,

$$[h_l(\hat{\mathbf{x}}_y \cdot \mathbf{n}) - \hat{\mathbf{x}}_y \cdot \mathbf{n}][h_r(\hat{\mathbf{x}}_y \cdot \mathbf{n}) - \hat{\mathbf{x}}_y \cdot \mathbf{n}] < 0, \tag{25}$$

where $(\cdot)$ denotes the inner product, and

$$\mathbf{n} \triangleq [1 \quad 0 \quad 0 \quad 0 \quad 0]^T. \tag{26}$$

Another set of constraints to be imposed on the lateral controller consists of the upper and lower bounds on the steering angle, such that

$$\delta_{\min} \leq \delta \leq \delta_{\max}. \tag{27}$$

As a result, the constrained optimal control problem for the design of the lateral RHC-based HDM is,

$$\min_{\mathbf{u}_y(t_0+k\Delta t)} J_y(\mathbf{u}_y, \mathbf{x}_y(t_0), t_c) \tag{28a}$$

subject to the set of equality and inequality constraints on the state and control,

$$\hat{\mathbf{x}}_y(t_0+(k+1)\Delta t) = \mathbf{A_d}\hat{\mathbf{x}}_y(t_0+k\Delta t) + \mathbf{B_d}\mathbf{u}_y(t_0+k\Delta t), \tag{28b}$$

$$\delta_{\min} \le \mathbf{u}_y(t_0+k\Delta t) \le \delta_{\max}, \tag{28c}$$

$$[h_l(\hat{\mathbf{x}}_y(t_0+(k+1)\Delta t)\cdot\mathbf{n}) - \hat{\mathbf{x}}_y(t_0+(k+1)\Delta t)\cdot\mathbf{n}] \times [h_r(\hat{\mathbf{x}}_y(t_0+(k+1)\Delta t)\cdot\mathbf{n}) - \hat{\mathbf{x}}_y(t_0+(k+1)\Delta t)\cdot\mathbf{n}] < 0, \tag{28d}$$

for $k = 0, \ldots, N-1$. Since J_y is a function of the future control inputs, the above constrained optimization will produce an optimal lateral control sequence denoted by $\mathbf{u}_y^*(t_0 + k\Delta t)_{k=0,\ldots,N-1}$.

A similar approach is utilized for designing the longitudinal controller, where the relation between two consecutive estimated states are obtained by integrating (18), such that

$$\hat{\mathbf{x}}_x(t_0+(k+1)\Delta t) = f(\hat{\mathbf{x}}_x(t_0+k\Delta t), \mathbf{u}_x(t_0+k\Delta t)). \tag{29}$$

The cost function is defined with respect to the target speed profile, $\mathbf{V}^*$,

$$J_x(\mathbf{u}_x, \mathbf{x}_x(t_0), t_c) = \|[\hat{\dot{x}}(t_0+\Delta t) \quad \ldots \quad \hat{\dot{x}}(t_0+N\Delta t)] - \mathbf{V}^*\|_2. \tag{30}$$

Upper and lower bounds for the engine torque and brake pressure are considered through the following inequality constraint on the control,

$$[T_{e_{\min}} \quad P_{b_{\min}} \quad 0]^T \le \mathbf{u}_x \le [T_{e_{\max}} \quad P_{b_{\max}} \quad 1]^T. \tag{31}$$

In addition, for ground vehicles, the engine torque and brake pressure should not act on the wheel simultaneously, therefore,

$$\det(\mathbf{C}\mathbf{u}_x + \mathbf{D}) = 0, \tag{32}$$

where $\det(\cdot)$ is the determinant of a matrix, and

$$\mathbf{C} = \begin{bmatrix} 1 & 0 & 0 \\ 0 & 1 & 0 \\ 0 & 0 & 0 \end{bmatrix}, \quad \mathbf{D} = \begin{bmatrix} 0 & 0 & 0 \\ 0 & 0 & 0 \\ 0 & 0 & 1 \end{bmatrix}. \tag{33}$$

Moreover, the driven mode indicator, γ should be either zero or one, which requires,

$$\mathbf{u}_x \cdot \mathbf{m} \in \{0, 1\}, \tag{34}$$

where

$$\mathbf{m} = [0 \quad 0 \quad 1]^T. \tag{35}$$

As a result, the constrained optimal problem for the longitudinal controller is,

$$\min_{\mathbf{u}_x(t_0+k\Delta t)} J_x(\mathbf{u}_x, \mathbf{x}_x(t_0), t_c) \tag{36a}$$

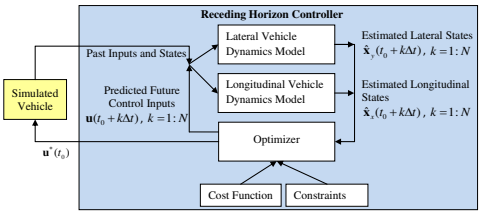

Fig. 4: Nonlinear receding horizon controller.

subject to the set of equality and inequality constraints,

$$\hat{\mathbf{x}}_x(t_0+(k+1)\Delta t) = f(\hat{\mathbf{x}}_x(t_0+k\Delta t), \mathbf{u}_x(t_0+k\Delta t)), \tag{36b}$$

$$[T_{e_{\min}} \quad P_{b_{\min}} \quad 0]^T \le \mathbf{u}_x(t_0+k\Delta t) \le [T_{e_{\max}} \quad P_{b_{\max}} \quad 1]^T, \tag{36c}$$

$$\det(\mathbf{C}\mathbf{u}_x(t_0+k\Delta t) + \mathbf{D}) = 0, \tag{36d}$$

$$\mathbf{u}_x(t_0+k\Delta t)\cdot\mathbf{m} \in \{0, 1\}, \tag{36e}$$

for $k = 0, \ldots, N-1$. Then, the solution of the above constrained optimization problem yields an optimal longitudinal control sequence, $\mathbf{u}_x^*(t_0+k\Delta t)_{k=0,\ldots,N-1}$.

B. ANN-based HDM

The ANN driver is obtained using a feed-forward sigmoidal neural network with the architecture shown in Fig. 5 and Fig. 6 [14] [15]. Sigmoidal neural networks have been shown capable of approximating nonlinear functions arbitrarily well, given a sufficient number of nodes [16] [17]. The Levenberg-Marquardt backpropagation algorithm is used to determine the network adjustable parameters, denoted by a matrix $\mathbf{W}$, from a set of training data obtained from experiments involving a professional human driver. A sample network layer is shown in Fig. 5. The neural network output is the control vector, $\mathbf{u}$, for driving the vehicle and the input vector, $\mathbf{p}$, as follows,

$$\mathbf{u} = \boldsymbol{\beta}[\mathbf{W}^{(l)}\mathbf{p}^{(l)} + \mathbf{d}^{(l)}], \tag{37}$$

$$\mathbf{p}^{(j)} = \boldsymbol{\sigma}^{(j)}[\mathbf{W}^{(j-1)}\mathbf{p}^{(j-1)} + \mathbf{d}^{(j-1)}], \tag{38}$$

where l is the number of neural network layers. $\mathbf{W}^{(j)}$ denotes the matrix of weights associated with the jth hidden layer, where the element $\mathbf{W}^{(j)}[i,k]$ represents the weight of the connection from the ith node in layer $(j-1)$ to the kth node in layer j. The vector function

$$\boldsymbol{\sigma}^{(j)} = [\sigma_1^{(j)}(s_1^{(j)}) \quad \ldots \quad \sigma_{n_j}^{(j)}(s_{n_j}^{(j)})]^T \tag{39}$$

contains n_j repeated transfer functions, $\sigma_i^{(j)}(\cdot)$, where n_j is the number of nodes in the jth layer, and $s_i^{(j)}$ is the weighted sum of the inputs to the ith node in the jth layer, for $i = 1, \ldots, n_j$. In this paper, it is assumed that all transfer functions are defined as the hyperbolic tangent,

$$\sigma_i^{(j)}(s) = \frac{\sinh(s)}{\cosh(s)}. \tag{40}$$

The number of nodes required is determined by trial and error. The linear vector function,

$$\boldsymbol{\beta} = [\beta_1(\mathbf{p}^{(l)}) \quad \ldots \quad \beta_{n_l}(\mathbf{p}^{(l)})]^T, \tag{41}$$

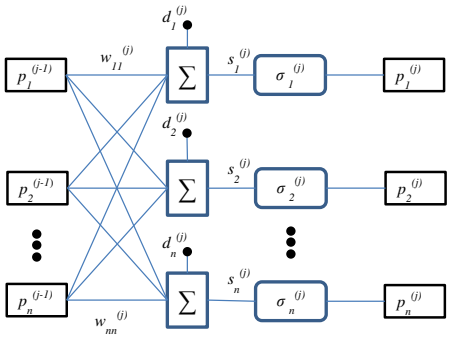

Fig. 5: Diagram of jth hidden layer.

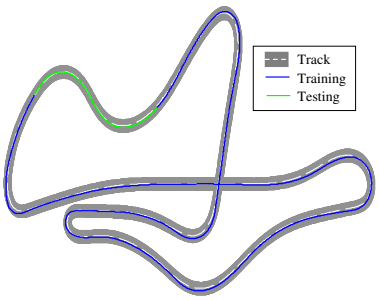

Fig. 7: Track used to collect the human driver data.

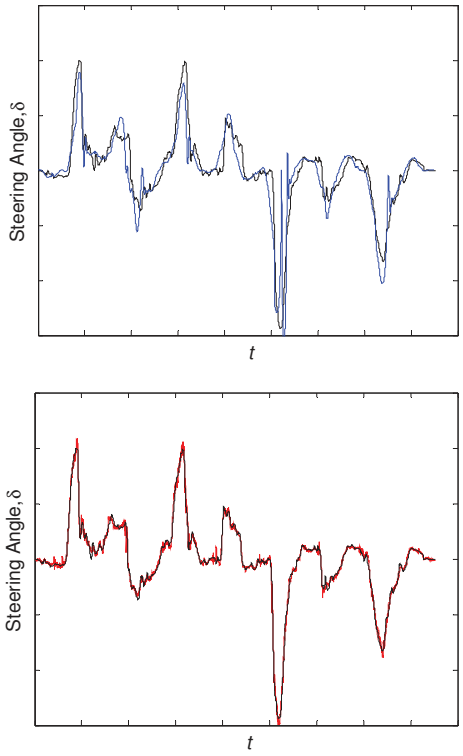

Fig. 8: Lateral controller performance comparison (scale and units are omitted to safeguard proprietary data).

is used to obtain the control input, $\mathbf{u}$, from the output vector of the last hidden layer, $\mathbf{p}^{(l)}$, where

$$\beta_i(\mathbf{p}^{(l)}) = \mathbf{b}_i \cdot \mathbf{p}^{(l)} + d_i^{(l)}, \tag{42}$$

and $\mathbf{b}_i$ is a vector of n_l weights, such that

$$\mathbf{d}^{(j)} = [d_1^{(j)} \quad d_2^{(j)} \quad \dots \quad d_{n_j}^{(j)}]^T \tag{43}$$

represents the jth hidden-layer bias vector.

The professional Ferrari GT simulator generates driver-input/vehicle-output pairs that are used to train the ANN. The professional human driver provides inputs to the Ferrari GT vehicle based on his expert knowledge of the optimal trajectory and velocity profiles for the track in Fig. 7. The training data consists of 8500 pairs of human driver control input values $\mathbf{u}_h = [\eta \quad P_c \quad G \quad \lambda \quad \delta]^T$, vehicle state values $\mathbf{x} = [\dot{x} \quad \ddot{x} \quad RPM]$, and target driver line values Γ^*, where λ and η are the percentages of brake and accelerator, respectively, P_c is the percentage of clutch engagement, and G is the gear. The training data is obtained from the blue portion (75%) of the track in Fig. 7, and a set of validation data is obtained from the green portion (25%) of the track in Fig. 7, which is never used for training. The driver line Γ^* is a vector of coordinate pairs representing the future target positions for the center of gravity of the vehicle over the control horizon t_c. Figure 6 illustrates the input/target values for the ANN-based HDM.

V. Simulation and Results

In this section the behaviors of both the RHC-based HDM and the ANN-based HDM are compared to the behavior of a professional human driver that is recorded on a high-fidelity Ferrari GT simulator. The Ferrari GT simulator provides the human driver, the ANN-based HDM, and the RHC-based HDM with the same information of the track and the vehicle. Additionally, this simulation of the GT vehicle closely matches the dynamic properties of real Ferrari GT vehicles. The same track, with the same start line and finishing line, is adopted for all the experiments. For HDMs, the driver line, Γ^*, is specified by the recorded trajectory of the vehicle in $\mathscr{F}_0$, which, in this paper, is generated by the human driver. Since the goal of the controllers is to mimic the response of the professional human driver, the recorded trajectory and speed profile can be considered as the optimal target trajectories to follow for the given track. All the experiments are conducted using the two-wheel-driven mode, with $\gamma = 0$.

Figure 8 shows the steering angle produced by the real human driver (black), the RHC-based HDM (blue), and the ANN-based HDM (red). The root-mean-squared (RMS) error between the RHC-based HDM response and the human driver response is 1.10×10^{-3}. The ANN-based response produces a RMS error of 1.97×10^{-4}. It can be seen that the ANN-based HDM generates outputs that are closer to the driver response, and thus the ANN-based HDM provides a better representation of human driver behavior.

Similar results are obtained for the longitudinal controller. Figure 9 shows that both the RHC-based HDM and the ANN-based HDM are capable of generating control inputs

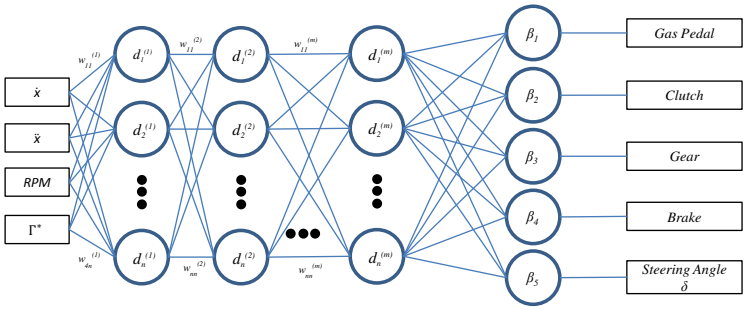

Fig. 6: Diagram of human driver model.

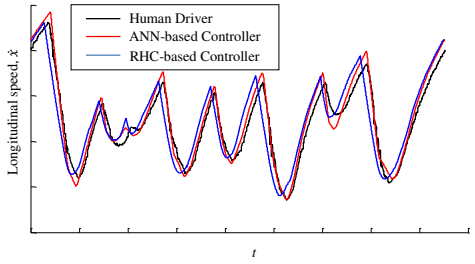

Fig. 9: Speed profiles generated by the human driver (black), the ANN-based HDM (red), and the RHC-based HDM (blue).

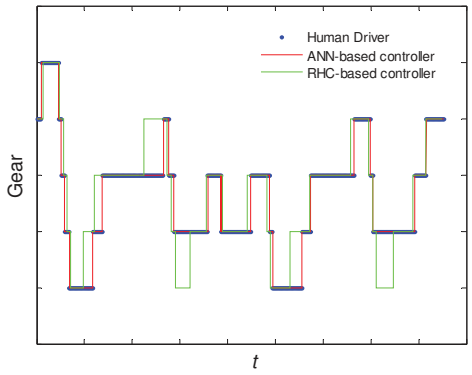

Fig. 10: Gear profiles generated by the Human Driver, RHC, and ANN

that allow the simulated vehicle to follow the target speed profile, $\mathbf{V}^*$, within a reasonable error. The RHC RMS error is 2.60×10^{-3} and the ANN RMS error is 1.60×10^{-3} for this particular test. However, when it comes to how well the HDMs represent the human driver's behavior, the results are much different. Figure 11 shows that the gas pedal percentage recorded from the human driver (black) while accelerating displays an RMS error of 2.50×10^{-4} when compared to the ANN-based HDM (red) and an RMS error of 3.70×10^{-3} when compared to the RHC-based HDM (blue). Also, Fig. 12 shows that, for the gas pedal percentage recorded from the human driver, the ANN-based HDM displays an RMS error of 2.77×10^{-4}, while the RHC-based HDM displays an RMS error of 2.10×10^{-3}.

All of the simulation results show that while both the RHC-based HDM and the ANN-based HDM are capable of generating commands that enables the simulated vehicle to follow the target trajectory within a reasonable error, the ANN-based HDM outperforms the RHC-based HDM in representing the driver behavior thanks to the ANN's ability to learn from the experimental data obtained from a human driver.

VI. Summary and Conclusion

This paper presents a comparison between ANN-based and RHC-based HDMs for the purpose of representing the behavior of a professional human driver in charge of controlling a Ferrari GT vehicle during coupled lateral-longitudinal maneuvers. The RHC-based design is obtained using a bicycle model for vehicle dynamics as well as the driver line, the speed profile, and the track information. The ANN-based design is obtained using a multi-layer sigmoidal neural network trained using a standard Levenberg-Marquardt algorithm with data generated by the professional human driver. The results show that the ANN-based HDM is better able to capture the human driver behavior than the RHC-based HDM is, because it learns from the experimental data obtained from the driver. In addition, designing the ANN-based HDM does not require a mathematical model of the vehicle dynamics and therefore does not require expert human intervention. As a result, tuning the ANN-based HDM to different drivers, automobiles, and road conditions is easier than tuning the RHC-based HDM. It can be concluded that the ANN-based HDM may some day be applied to enhance the efficiency of automobile manufacturing, for example by reducing the delivery time and cost or by enabling vehicle safety and performance testing through extensive simulations.

VII. Acknowledgements

This material is based upon work supported by the National Science Foundation under Grant No. DGE-1068871.

References

[1] P. Falcone, M. Tufo, F. Borrelli, J. Asgari, and H. Tseng, "A linear time varying model predictive control approach to the integrated vehicle dynamics control problem in autonomous systems," in *Decision and Control, 2007 46th IEEE Conference on*, dec. 2007, pp. 2980 –2985.

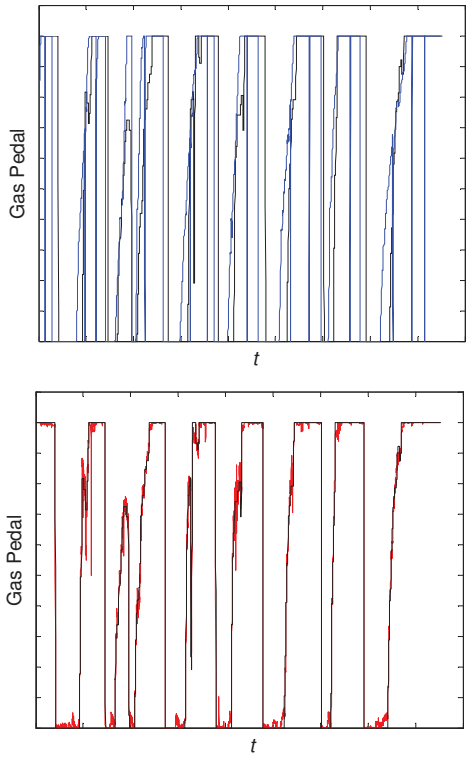

Fig. 11: Gas pedal command generated by the human driver (black), the ANN-based HDM (red), and the RHC-based HDM (blue).

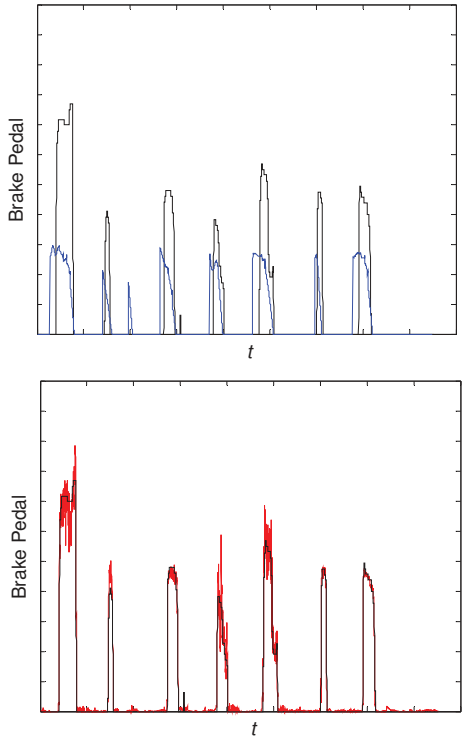

Fig. 12: Brake pedal command generated by the human driver (black), the ANN-based HDM (red), and the RHC-based HDM (blue).

[2] V. Akpan and G. Hassapis, "Adaptive predictive control using recurrent neural network identification," in *Control and Automation, 2009. MED '09. 17th Mediterranean Conference on*, june 2009, pp. 61 –66.

[3] R. Hess and A. Modjtahedzadeh, "A control theoretic model of driver steering behavior," *Control Systems Magazine, IEEE*, vol. 10, no. 5, pp. 3–8, Aug 1990.

[4] B. Schofield, T. Hagglund, and A. Rantzer, "Vehicle dynamics control and controller allocation for rollover prevention," in *Computer Aided Control System Design, 2006 IEEE International Conference on Control Applications, 2006 IEEE International Symposium on Intelligent Control, 2006 IEEE*. IEEE, 2006, pp. 149–154.

[5] A. Y. Ungoren and H. Peng, "An adaptive lateral preview driver model," *Vehicle System Dynamics*, vol. 43, no. 4, pp. 245–259, 2005.

[6] T. D. Gillespie, "Fundamentals of vehicle dynamics," 1992.

[7] H. Pacejka, *Tyre and vehicle dynamics*. Butterworth-Heinemann, 2005.

[8] V. Cossalter, *Motorcycle dynamics*, 2006.

[9] C. C. Macadam, "Understanding and modeling the human driver," *Vehicle System Dynamics*, vol. 40, no. 1-3, pp. 101–134, 2003.

[10] S. Ferrari, "Multiobjective algebraic synthesis of neural control systems by implicit model following," *Neural Networks, IEEE Transactions on*, vol. 20, no. 3, pp. 406–419, 2009.

[11] D. Q. Mayne and H. Michalska, "Receding horizon control of nonlinear systems," *Automatic Control, IEEE Transactions on*, vol. 35, no. 7, pp. 814–824, 1990.

[12] T. Kailath, *Linear systems*. Prentice-Hall Englewood Cliffs, NJ, 1980, vol. 1.

[13] M. Bertozzi and A. Broggi, "Gold: A parallel real-time stereo vision system for generic obstacle and lane detection," *Image Processing, IEEE Transactions on*, vol. 7, no. 1, pp. 62–81, 1998.

[14] S. Russell and P. Norvig, *Artificial Intelligence A Modern Approach*. Upper Saddle River, NJ: Prentice Hall, 2003.

[15] F. L. Lewis, S. Jagannathan, and A. Yesildirek, *Neural Network Control of Robot Manipulators and Nonlinear Systems*. Taylor & Francis, 1999.

[16] G. Cybenko, "Approximation by superpositions of a sigmoidal function," *Mathematics of Control, Signals and Systems*, vol. 2, no. 4, pp. 303–314, 1989. [Online]. Available: http://dx.doi.org/10.1007/BF02551274

[17] S. M. Carroll and B. Dickinson, "Construction of neural nets using the radon transform," in *Neural Networks, 1989. IJCNN., International Joint Conference on*, 1989, pp. 607–611 vol.1.